Soft Matter

PAPER

View Article Online
View Journal | View Issue

Cite this: *Soft Matter*, 2026, **22**, 1630

Drug & virus transport across biological barriers: interactions, diffusion, partitioning, permeability, and selectivity

Mikael O. Ellingson and Michael A. Bevan *

Biological barriers protect the human body by selectively blocking foreign material. Designing particles with coatings that efficiently transport across these barriers can increase the effectiveness and feasibility of advanced therapeutics. In particular, the mucus barrier protects the intestines, lungs, eyes, *etc.*, complicating oral, inhaled, or ocular drug delivery. Heuristics for particle design are currently limited to the rate of diffusion within the barrier. Relying on first-principles theories for colloidal scale interactions, a cohesive model of the transport of particles through biological barriers is developed based on the barrier permeability, which incorporates essential contributions from both partitioning and diffusion. Analytical models are developed to predict partition coefficients based on particle–pore interaction potentials. Particle–pore hydrodynamics are considered to predict average diffusivities within mucus barriers. We show that kT-scale attractive interactions, that are either specific or non-specific, can yield optimal delivery of larger particles, to increase the mass flux across mucus barriers by an order of magnitude, and enable delivery of macromolecular cargo, due to enhanced partitioning. Our model indicates drug particle design rules to achieve transport rates comparable to or exceeding what is possible by viruses with highly evolved chemical and physical characteristics.

Received 25th November 2025,
Accepted 29th January 2026

DOI: 10.1039/d5sm01176k

rsc.li/soft-matter-journal

Introduction

Drug delivery necessitates transporting material across biological barriers.[1] The blood–brain barrier, extra-cellular matrix, vascular walls, epidermis, and mucosal barriers all present barriers to pathogens but also provide routes for delivery of molecular and colloidal species.[2–4] Particles that efficiently cross these barriers are necessary for therapeutics and diagnostics; *e.g.*, encapsulated mRNA has been used for vaccination against COVID19,[5] and designed nanoparticles could be used for a broad range of precision therapeutics and diagnostics.[6] The mucus barrier is highly selective[7] due to a matrix of mucin fibers,[7,8] trapping some virus particles.[9] Adding PEG macromolecular layers to make the particles "stealth" or "mucopenetrating" has been a popular strategy, increasing the rate of diffusion within mucus,[10,11] but with limited overall success.[12] On the other hand, virus particles with hindered diffusivities nevertheless infect hosts.[9,13] Drug and virus particles both undergo Brownian motion, have surface coatings that determine transport efficacy, and are optimized for payload delivery. A generalized prediction for transport through biological barriers in general and mucus in particular would shed light on virus and drug transport allowing for the improved design of drug coatings.[14]

The transport of solute across barriers is generally characterized by the permeability,[15–24] which is used to quantify the total amount of mass crossing the barrier. Generally, permeabilities are comprised by partition and diffusion coefficients,

$$P = KD \tag{1}$$

where P is the solute-barrier permeability, and K and D are the partition and the diffusion coefficients. K captures the thermodynamic driving forces for particles to enter into barriers, and D reflects the rate of the random Brownian motion of particles within the barrier. Modeling permeabilities has been applied in descriptions of transport at the molecular[15–17] and colloidal[18–26] scales. Previous applications of permeabilities to biological barriers has been limited to lipid bilayers[19,20] and the skin.[27] Modeling of the transport through mucus barriers is often limited to include only the diffusive contribution (*i.e.*, $K = 1$).[28] Indeed, most measurements of drug particles in mucus are of diffusion alone,[8,29] which narrows the focus of drug particle optimization.[30]

Partitioning has been hypothesized to be important for viral infection,[9] and for engineering drug particles,[4] because it encourages particles to enter the barrier. Viral transport involves attractive specific interactions.[31–33] However, discussion of the

Chemical & Biomolecular Engr., Johns Hopkins Univ., Baltimore, MD 21218, USA. E-mail: mabevan@jhu.edu

effect on drug delivery is limited to qualitative descriptions.[4] The earliest quantitative predictions of partitioning was of the free space in random fiber matrices for gel chromatography.[34,35] These excluded volume effects change the entropy and free energy differences for particles inside and outside barrier pores, and thereby the transport across barriers.[36] Incorporating free energy differences allowed the partitioning calculations to be generalized to any particle–pore interactions,[37,38] which has been validated in limited cases (*e.g.*, macromolecules in fibrous media[39]). The calculation of the partition coefficient requires the geometry of the medium, and most analyses involve idealized cylindrical pore geometries,[40] including biological barriers.[41] In contrast, explicit fibers models require more extensive modeling and do not lead to closed-form solutions.[18,37,38] The deviations between these approaches are negligible until the particle approaches the mesh size.[42] Despite the importance of partitioning, predictions have yet to be applied to mucus barrier permeation.

The effect of diffusivity on the transport is well known in the mucus drug delivery literature.[4,9,43] One quantitative approximation is to use an effective medium approach,[23,44–46] inferring averaged hydrodynamic friction on particles from measurements over short times.[23] However, these effective media results cannot be used to model and distinguish localization effects from energetic interactions.[47] While localization could be captured by averaging the position dependent mobility with the probability of observing that state,[48–51] this has not been applied to barrier transport models. Furthermore, reversible binding is known to affect measured average diffusivities,[52,53] which has been observed with viral transport,[54] and could be averaged along with other the non-specific effects.[55] Similar to partitioning, models of the medium geometry are required, with explicit fibers or ideal pore models being used.[46] Explicit fiber models require fiber distributions and particle–fiber hydrodynamics,[42,52,56] both of which lead to expensive calculations and limited applicability. Effective pore models have been applied to the diffusion of macromolecules in fibrous matrices[57–59] and the dynamics of long, flexible solutes in hydrogels.[60–62] Measurements and models of the hydrodynamic interaction have been considered for colloidal particles in slit-pores[22,63–67] and cylindrical pores.[68–70] However, models for the position dependent diffusivity of spherical colloids within cylindrical pores due to hydrodynamic interactions are limited to the centerline and do not include effects of colloidal interaction potentials.[71]

Particle interactions on the *kT*-scale mediated by solution and surface chemistry also affect particle diffusivity and partitioning,[7,9,72] by changing localization, confinement, and/or potential energy contributions to the overall system free energy. Due to the high ionic strength of biological media, electrostatics are highly screened and have negligible effects at the colloidal scale.[49] The governing colloidal scale interactions are van der Waals attraction,[73,74] macromolecular repulsion[43,49,73,75] and specific biomolecular interactions,[73,76,77] all of which have been measured and modeled at the colloidal scale. The Derjaguin approximation enables specification of realistic interaction potentials in systems with arbitrary curvature in models of van der Waals, macromolecular coatings, *etc.*[78] Non-specific osmotic repulsion between particle coatings and mucin fibers tends to stabilize particles against aggregation and deposition and increase surface separation.[10,79,80] Specific interactions arise from molecular scale interactions,[81] *e.g.*, the formation of dynamic covalent bonds with mucin sialic acids.[82] Applying these models to predictions of partitioning and diffusion would allow for the prediction of transport from fundamental surface properties.

In this paper, we report a model for colloidal transport across biological barriers with systemic delivery through mucus barriers as a specific example target (Fig. 1A). This model focuses on the transport of particles into and through mucus barriers (Fig. 1B), which is modeled as pores within fibrous matrices (Fig. 1C), with the goal of capturing dominant effects of particle–fiber interactions. It captures the effects of *kT*-scale particle–pore surface interaction potentials (U) on partitioning (K) and hindered diffusion (D), and prediction of the permeability (P) and mass flux through the mucus barrier (Fig. 1D). In this way, particle interactions controlling transport across biological barriers can be modeled with the goal of optimizing particle size and coating mediated interactions, including comparisons against virus transport (Fig. 1E).

Theory

Particle flux across barriers

Fick's laws predict the flux of solutes through a barrier as being proportional to spatial concentration gradients,[46] where for films at steady state (see SI),

$$j = PC\rho/l \tag{2}$$

where j is mass flux across the barrier, C is the concentration difference, ρ is the mass density per particle, l is barrier width, and P is barrier permeability (see eqn (1)). Note that tortuosity and porosity effects could be incorporated as an order-unity multiplicative factor to permeability[46] but are not captured here. The corresponding transient solution has been derived,[83] with deviations captured by a multiplicative factor to eqn (2) (see SI). This transient solution predicts that the concentration in the barrier evolves as,

$$\begin{aligned}\frac{C_{\mathrm{B}}(t)}{C_{\mathrm{L}}} &= \frac{C(z=l,t)}{KC_{\mathrm{L}}} \\ &= K^{-1}\left[1-2\sum_{n=1}^{\infty}\frac{\left(H^2+Q_n^2\right)\sin(Q_n)}{\left(H+H^2+Q_n^2\right)Q_n}\exp\left(-DQ_n^2t/l^2\right)\right]\end{aligned} \tag{3}$$

where $C_{\mathrm{B}}(t)$ is the transient concentration of drug in the blood, C_{L} is the constant concentration of the drug in the lungs, $C(z,t)$ is the concentration profile in the mucus, and H and Q_n are factors that depend on the relative volumes of the mucus and blood compartments.

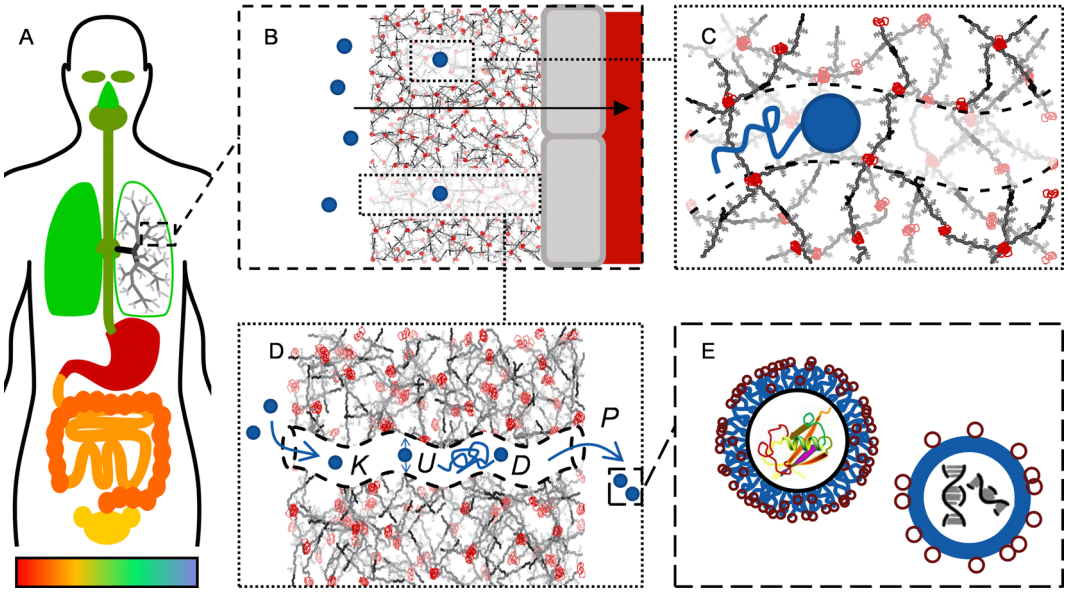

Fig. 1 Multiscale diagram showing mucus barriers and transporting particles. (A)–(D) Diagrams of mucus barriers. (A) Mucus barriers all over the body with various pH values (highly acidic, red/orange; basic, blue-green), with details of the branching bronchial passages in the lungs and dashed callout to B. (B) Detail of the mucus layer, with a dense mucin matrix with pores leading to an epithelial layer, with dashed callout to C. (C) Pore-scale detail of the mucus membrane, showing idealized pores passing through random matrix. (D) Overall transport process, involving partitioning, *K*, particle–pore interactions, *U*, in-pore particle diffusivity, *D*, and overall permeability, *P*; dashed callout to E. (E) Drug (top) and virus (bottom-right) particles, with loaded cores (*e.g.*, insulin or genetic material).

Particle-pore potential energies

Particles interact with pore walls with net position dependent interactions, $U(r)$, given by the superposition of contributing potentials as,

$$U(r) = U_H(r) + U_S(r) + U_V(r) + U_{RL}(r) \quad (4)$$

where U_H is a hard-wall interaction, U_S is a steric interaction, U_V is a van der Waals interaction, and U_{RL} is a specific receptor–ligand interaction. The inability of particles to penetrate surfaces is given by a hard-wall potential, which also provides a useful reference state,[37] as given by,

$$U_H(r) = \{\infty, \quad r \le R - a, \quad \text{else } 0 \quad (5)$$

where R is the radius of the circular pore, and a is the particle radius. Macromolecular layers upon contact generally experience compression-dependent free-energies, which can be integrated using the Derjaguin approximation[75] or sphere-pore geometries as,

$$U_S(r) = \Gamma a(1 - a/R)^{-1/2} \exp(-\gamma[R - a - r]) \quad (6)$$

where Γ and γ are related to the free energy and length of uncompressed brushes, $\gamma = 5.2/L$ (see SI).[75] van der Waals attraction can be expressed for particles small compared to pore dimension by Hamaker integration, to yield a particle–pore potential. An additional correction can be obtained from matching an exact integration for particle–pores,[84] which improves the approximation for int the limit of particles approaching the pore size,

$$U_V(r) = Aa/66(R/a - r/a)^{-1}(1 - a/R)^{-1/2}(R - a - r)^{-1} \quad (7)$$

where A is the Hamaker constant for the particle–pore materials (see SI). Receptor–ligand interactions are reversible specific interactions between chemical species on the particle and fiber surfaces.[76] Various approximations of receptor–ligand interactions are available including harmonic wells that capture contact forces,[76,85] but for simplicity and applicability to thermodynamic analyses relevant to partition coefficients, adhesive spheres with only contact energies can be suitable, as given by,

$$U_{RL}(r) = \{-|U_M|, \quad R - a - r \le L, \quad \text{else } 0 \quad (8)$$

where U_M is the binding strength of the receptor–ligand interaction.

Distribution of colloids at interfaces: partition coefficients

Partition coefficients are calculated to consider contributions from entropy and potential energy as separable quantities. Entropic contributions can be captured by considering solely hard particle–pore interactions,[37] which simplifies to geometry dependent available (not excluded) volumes.[34,37,86] Potential energy contributions to the partitioning coefficient are captured by an additional term given by (see SI),

$$K = K_{HS} + K_U = (1 - a/R)^2 + \frac{2}{R^2}\int_0^{R-a} [\exp(-U(r)/kT) - 1] r dr \quad (9)$$

where K_{HS} and K_U are partitioning due to hard-sphere and other colloidal potentials (where k is Boltzmann's constant and T is absolute temperature). For not-dilute colloidal dispersions with repulsive pair interactions, partitioning can be enhanced by higher particle concentrations.[39]

Diffusion & hydrodynamic interactions

The average particle diffusivity within pores can be modeled to include hydrodynamic interactions and how particles sample the potential energy landscape within pores, which is given by a Boltzmann weighted average of separation dependent hydrodynamic interactions as,[49]

$$D = \int D_{\parallel}(r)p(r)r\mathrm{d}r \tag{10}$$

where $D_{\parallel}$ is the diffusivity of a spherical particle parallel to the pore central axis or walls, and $p(r)$ is the normalized Boltzmann distribution of a colloid in an energy well, $p(r) = \exp[-U(r)/kT]/\int\exp[-U(r)/kT]\mathrm{d}r$. Although the $D_{\parallel}$ along the centerline of cylindrical pores is known,[87] exact results are not known for arbitrary positions within pores.[68,70] For a simple approximation of size- and position- dependent diffusivities based on known limits, a linear interpolation (based on the linear lubrication asymptote) between the centerline[87] and wall contact results gives the form (see SI),[88]

$$D_{\parallel}(r,a_{\mathrm{H}},R) = D_0H_{\parallel,\mathrm{c}}(r,a_{\mathrm{H}},R) = D_0[(f_{\parallel,\mathrm{c}}(a_{\mathrm{H}},R) - 0.32)(R - a_{\mathrm{H}} - r)/(R - a_{\mathrm{H}}) + 032] \tag{11}$$

where $H_{\parallel,\mathrm{c}}$ is the hydrodynamic mobility of the particles along the cylindrical axis and $D_0 = kT/6\pi\mu a_{\mathrm{H}}$ is the single particle diffusivity far from any boundaries, where μ is medium viscosity, and a_{H} is the particle hydrodynamic radius given by a hard–core radius plus a fraction (ϕ) of the polymer layer thickness given as,[49]

$$a_{\mathrm{H}} = a + [1 - \phi]L \tag{12}$$

Results & discussion

Particle-pore interaction potentials

The colloidal interactions between particles and mucus pores are analyzed first since they contribute to all aspects of barrier transport including partitioning, diffusion, permeation, and selectivity. Particles in mucus barriers are approximated as moving along cylindrical pores where particles are in close proximity to the pore walls as dictated by their size and interactions (Fig. 2A). As a result, there is a need to describe the colloidal interactions of particles with the porous matrix itself as particles tend to localize at potential energy minima. Considering that respiratory mucus barriers are generally of order ~10 μm in thickness[7] with pore sizes of ~400 nm, which are 2 orders of magnitude smaller,[13] end effects are considered to be negligible.[19]

We first consider particles with no long-range interactions where only hard-wall interactions (eqn (5)) preclude particle–wall overlap (black curve Fig. 2B). Particles with such interactions equally sample all positions due to a uniform zero interaction everywhere except with an infinite interaction on contact with pore walls. Additionally, we consider exponential potentials that are representative of electrostatic and steric interactions and show key features of longer-range soft interactions in addition to hard core potentials. Repulsive interactions lead to high energies near the walls and a minimum at the centerline of the pore, where particles are localized (B = 1–100kT, blue, Fig. 2B). However, attractive interactions yield minima at the walls, localizing particles into those regions (B = −(2–4)kT, red, Fig. 2B). By adding exponential interactions to hard-wall potentials, particles sample different positions within pores to different degrees and have different overall free energies within pores compared to outside pores.

In addition to model hard-wall and exponential potentials, we also consider realistic first principles analytical models of particle–pore potentials (eqn (4)) including combinations of polymer brush repulsion, van der Waals attractions, and specific receptor–ligand interactions. These interactions lead to a minimum near the wall, that is mitigated by increasing brush length (A = −3kT nm^{-1}, L = 10–30 nm, Γ = 1.2kT nm^{-1},[49] cyan, Fig. 2B). With specific receptor–ligand attraction (L = 20 nm, $|U_{\mathrm{M}}|$ = 0.5–1.5kT, red, Fig. 2C), the minimum is deepened and

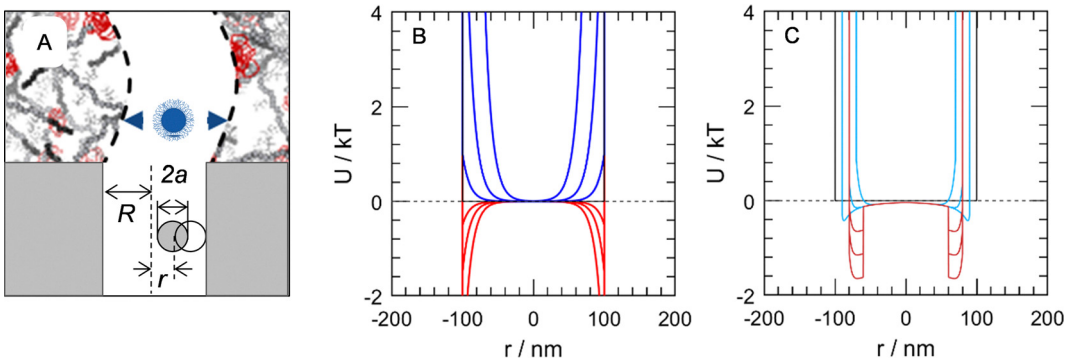

Fig. 2 Particle–pore energetic interactions. (A) Diagram of particles (blue/grey circles) interacting with pore walls (grey) with annotated pore size, R, particle size, 2a, and particle position, r. Outlined particle is in contact with the wall. (B) and (C) Particle–pore potential energies from models (eqn (4)), compared to the hard-sphere potential (solid black). Potentials are mirrored along r = 0 for clarity; only the r > 0 profile is used in calculations. (B) Attractive exponential potentials $U(r) = B\exp(-\kappa(R - a - r))$ potentials (B < 0, blue) compared to repulsive potentials (B > 0, red); B = −4, −3, −2, +1, +10, +100kT; κ^{-1} = 10 nm. (C) Model potentials (eqn (4)) with van der Waals (A = −3kT), steric interactions & receptor–ligand superposition (dark red, L = 20 nm, $|U_{\mathrm{M}}|$ = 0.5–1.5kT), compared to no specific attractions (cyan, L = 10, 20, 30 nm).

extended further from the wall (red, Fig. 2B). The superposition of these potentials leads to a steep repulsion at the wall from osmotic repulsion in all cases. While all designs modeled here localize the particles close to the pore wall, the specific attraction forms a well at the onset of the specific attraction, rather than at appreciable brush compression. Overall, the different surface coating designs present different particle localization within pores *via* the modeled free energy landscapes (energy *vs.* position in Fig. 2B and C).

Particle partitioning into barrier pores

Having developed particle–pore interaction potentials (Fig. 2), the next step is prediction of particle partitioning from unbounded bulk media into pores (eqn (9), Fig. 3A) based on changes in potential and free energies. The partitioning of hard-spheres into cylindrical pores can be predicted analytically (K_{HS} in eqn (9)) consistent with prior predictions.[37,39] In the limit of small particles ($a \rightarrow 0$), the particle has no interactions with the pore, leading to a partition coefficient of unity (inset of Fig. 3B). However, as particle size increases relative to pore dimensions, fewer microstates are available for particles within pores, which is associated with a decrease in entropy and increased free energy (potential energy does not change for hard-wall interactions in pores). Partitioning vanishes as the particle approaches the pore size, consistent with intuition.

Different realistic repulsive and attractive interactions in addition to hard–core interactions can be used to model and understand the effects of particle–pore interaction potentials on partitioning (Fig. 3B and C). In parallel with the presentation of interaction potentials in Fig. 2, we first consider effects on partitioning of the same soft exponential interaction potentials (Fig. 2B). Attractive potentials lead to enhanced partitioning for all sizes (red in Fig. 3B). Notably, the partitioning for small particles is much higher than for hard-wall particles. In contrast, repulsive potentials lead to hindered partitioning (blue in Fig. 3B). This hinderance can be around half the same sized hard–core particle, although it is apparently less sensitive to the magnitude of the exponential potential. Thus, kT-scale particle–pore interactions can significantly affect partitioning and ultimately impact permeation (as evident in eqn (1)), which will be discussed in the following.

Such enhanced partitioning can also be achieved by engineering realistic interaction potentials mediated by specific attractions between particle coatings and the mucus matrix, modeled with the same parameters as in Fig. 2C. In the small particle limit, there is a large enhancement from specific attraction, up to $\sim 4\times$ (red in Fig. 3C). As particles increase in size, the attraction does not change, but the decreased entropy and increased steric energy scale diminish the partitioning to vanish as particle size approaches pore dimensions. Similarly, particles with no specific attraction are only hindered, due to the steric interactions increasing free energy due to entropic and potential energy penalties (blue in Fig. 3C). Thus, the engineering of specific attractions on the kT-scale could lead to significantly enhanced partitioning to favor permeation.

Particle diffusivity within barrier pores

With an understanding of the effects of interaction potentials on partitioning, we next consider how interactions affect particle diffusivity within pores (Fig. 4A). Particles undergoing random Brownian motion within a crowded medium, such as mucus barrier pores, experience additional hindrance due to hydrodynamic interactions. The role of hydrodynamic interactions are captured for spherical particle within cylindrical pores based on best available solutions for rigorous asymptotic limits (eqn (11)). As already noted, particles sample different pore regions spatially according to interactions potentials (eqn (10)), so that they most frequently sample potential energy minima within the pore center for repulsive interactions or pore walls for attractive interactions. As a result, the average diffusivity is determined by hydrodynamic hindrance weighted by the relative sampling of different pore regions (eqn (10)). Different biological barriers, including fibrous media, may have varying degrees of hydrodynamic hinderance due to the ability of solvent to flow through pore walls. However, allowing for different spatial dependencies within pore is not the dominant effect for overall transport as will be shown in the following.

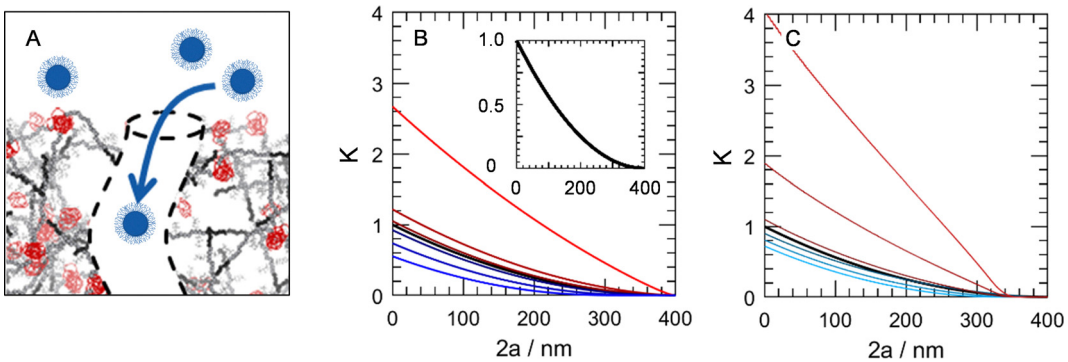

Fig. 3 Partitioning of particles into pores with different energy models. (A) Diagram of particles (blue/grey circles) entering into pores (grey). (B) and (C) Particle–pore partitioning from models (eqn (9)), compared to the hard-sphere partitioning (solid black, highlighted in B inset). (B) Partitioning due to exponential potentials with the same energy scale values/color scheme as Fig. 2. (C) Model potentials (eqn (4)) with the same parameters/color scheme as Fig. 2.

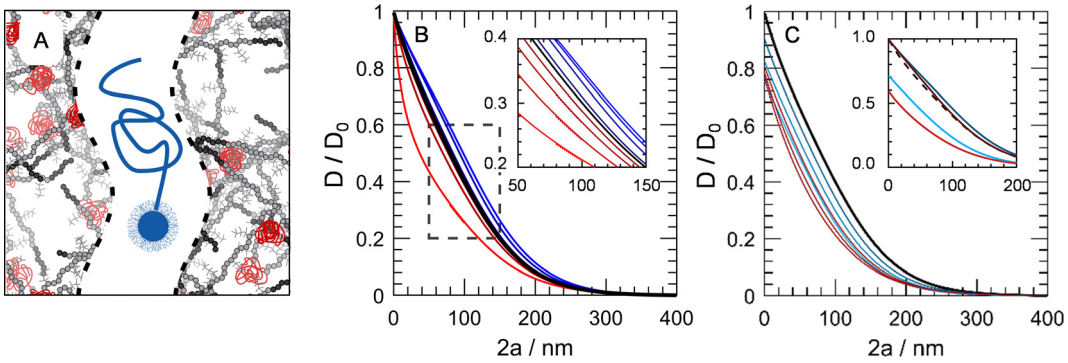

Fig. 4 In-pore particle diffusivity according to energetic models and polymer layer hydrodynamics. (A) Diagram of particles (blue/grey circles) undergoing random diffusion in pores (grey). (B) and (C) Particle diffusivity from models (eqn (10)), compared to the hard-sphere diffusivity (solid black). (B) particles with exponential potentials with the same energy scale values/color scheme as Fig. 2 and 3. Inset shows details of the box. (C) Model potentials (eqn (4)) with the same parameters/color scheme as Fig. 2 and 3. Inset shows comparisons of the longest brush length with impermeable layers (ϕ = 0, light colors) and fully permeable layers (ϕ = 1, dark colors). Hard-wall reference is shown dashed for clarity.

For hard-wall particle–pore interactions, particles sample all positions equally within the pore (black in Fig. 4B). It is most easy in this limit to demonstrate the effects of hydrodynamic interactions that depend on the relative particle and pore dimensions and on particle positions within pores. Because vanishingly small particles ($a \to 0$) are effectively in free space, the curve approaches D_0 in that limit. Additionally, as the particle approaches the pore size, hydrodynamic interactions in the lubrication limit diverge to yield an infinite resistance to particle motion, which produces a vanishing diffusivity. Together, these effects lead to a sublinear dependence on particle size for hard-wall particles.

We next consider the same colloidal interaction potentials and parameters as in Fig. 2B and 3B. Repulsive potentials (blue, Fig. 4B) tend to localize the particles near the centerline where the hydrodynamic friction is lowest. Thus, the diffusivity is faster than the hard particles. Attractive interactions (red, Fig. 4B) localize the particles near the pore walls, hindering particle motion due to increased hydrodynamic resistance. For these model interactions, the diffusivity spans at most a $\sim 0.2D_0$ difference in diffusivity at intermediate particle sizes (inset of Fig. 4B) because of the rolling diffusivity. As noted, explicit fiber models with varying degrees of finite fluid flow through the idealized pore walls, would predict a smaller localization effect, making the resistance due to localization a less significant factor compared to this model pore with impermeable boundaries.

We also consider how particle macromolecular coatings with varying solvent permeability can influence hydrodynamic resistance and particle diffusion within pores (inset of Fig. 4C). For particles with 20 nm brushes and either no specific interactions (cyan) or $-1.5kT$ well-depths (red) the diffusivity varies from the most hindered case with impermeable layers (light colors, ϕ = 0 in eqn (12)) to the core limit for particle with completely permeable layers (dark colors, ϕ = 1 in eqn (12)). The permeability of brushes have been experimentally measured, and they could feasibly be modified by changes to layers.[49] For the attractive case, where pore wall localization and effectively larger sizes both hinder the diffusivity, an increase in the polymer layer permeability can have significant effects on the particle diffusivity. Thus, brush-solvent permeability leads to a size- and localization-dependent increases in particle diffusivities within pores.

Most realistic particle coatings decrease the diffusivity in pores, either due to increasing the effective hydrodynamic size, or by localizing the particle near the wall. The model exponential repulsive interaction potential (*e.g.*, electrostatic repulsion) is the only case that results in faster diffusion than hard spheres, because it localizes the particle closer to centerline without an increase in hydrodynamic size. Particles with macromolecular coatings have repulsive interactions with pores diffuse faster than attractive interactions that localize particles near pore boundaries, consistent with measurements of PEG-coated particles.[10] This model can also explain the decreased diffusivity of longer polymer brushes, which has also been observed[10] (and previously perhaps mis-attributed to chain entanglement). The coupled effects of different interaction potentials and hydrodynamic interactions on particle diffusivities within pores can be well understood from first principles mechanisms and produce trends consistent with existing literature reports.

Barrier permeability & particle mass flux

Models of particle–pore interactions on both partition and diffusion coefficients can now be combined (eqn (1)) to understand their net effect on particle permeability across biological barriers including the specific example of mucus. The permeability is incorporated in a model of mass flux of particles across the barrier (eqn (10), Fig. 5A). Because mass flux is solely determined by how particle surface properties mediate interactions potentials (eqn (4)) and hydrodynamic interactions (eqn (11)), the effect of each can be determined. By considering the combined effect of interactions on both partitioning and diffusion, the essential material properties of particle coatings can be optimized in an informed manner to design drug particle coating for maximum transport across barriers.

Important limits of mass flux are demonstrated by first considering the case of hard spheres. There is no mass flux in

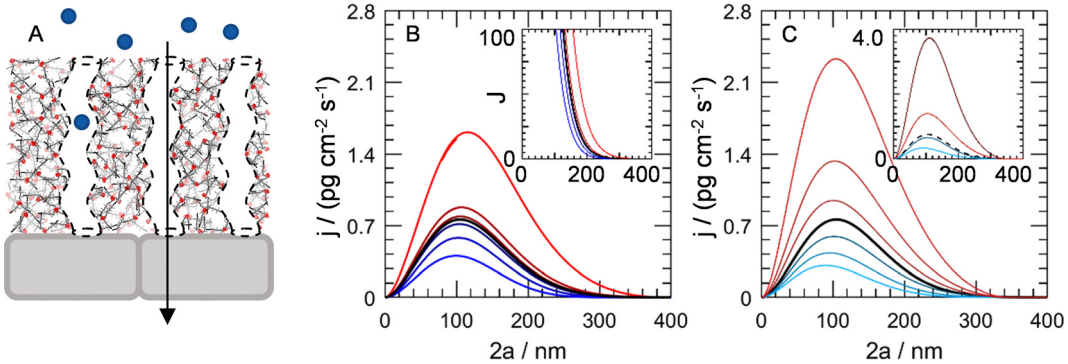

Fig. 5 Prediction of fluxes through mucus barriers. (A) Diagram of transport through the mucus barriers (grey). (B) and (C) Mass flux from models (eqn (10)), compared to the hard-sphere mass flux (solid black). (B) Particles with exponential potentials with the same energy scale values/color scheme as Fig. 2–4. Inset shows number flux (cm^{-2} s^{-1}) for the same interactions. (C) Model potentials (eqn (4)) with the same parameters/color scheme as Fig. 2–4. Inset shows the corresponding flux comparison with permeable (dark)/impermeable (light) layers as Fig. 4.

two circumstances. First, for particles approaching zero size ($a \rightarrow 0$), there is no mass to transport (Fig. 5B). Second, as particles approach the pore size, the partitioning (Fig. 3) and diffusivity (Fig. 4) coefficients both tend to zero due to unfavorable partitioning *via* a purely entropic penalty as well as hydrodynamic resistance resulting in a vanishing diffusivity. Between these limiting cases, an optimal size is observed to produce a maximum mass flux for hard-sphere particles at $2a \approx 100$ nm (Fig. 5B). It is interesting to note this is near the characteristic dimension of many viruses.[9]

With the addition of attractive and repulsion particle–pore interaction potentials, there is enhancement or hinderance from relative to the hard-sphere core particles of the same dimension. For repulsive potentials (blue, Fig. 5B), the partitioning is hindered to a larger degree than the diffusivity is enhanced. Thus, repulsive potentials produce mass fluxes for all particle sizes that are less than the corresponding hard sphere flux. Conversely, for attractive potentials (red, Fig. 5B), the enhanced partitioning, and thus permeability, leads to increased mass flux by nearly an order of magnitude. Thus, while partitioning and diffusivity are both integral to permeability, partitioning effects due to *kT*-scale attractive interactions have net enhancing effects.

Because the functional goal of drug delivery is to deliver the most mass of drug to the desired site, the mass flux has been reported. Note that while one could also consider the number flux, *i.e.*, the number of particles passing through the barrier, it is less important than the mass flux. The number flux has a simple, monotonic relationship with particle size (inset of Fig. 5B). This hides the trend capturing the mass per particle and thus increased delivery. The same trends according to surface properties can be interpreted from the number flux series. However, for the overall optimization, mass flux corresponds to better delivery strategies. Increasing drug particle size increases in proportion the mass flux of either small molecule or macromolecular cargo and could enable critical particle sizes necessary to encapsulate larger macromolecular therapeutics (*e.g.*, proteins, nucleic acids, multimers, *etc.*).

We consider next the realistic potential models incorporating realistic engineered and specific interactions. Using the same models as Fig. 2–4, the mass flux of particles with only brush layers ($U_M = 0$) is diminished (blue in Fig. 5C) relative to hard spheres, due to the combined effects of hindered partitioning and diffusivity (*cf.*, Fig. 3C and 4C). For attractive receptor–ligand interactions ($U_M \neq 0$), interaction strengths on the *kT*-scale can lead to enhanced partitioning and thus effective transport (red Fig. 5C). Engineered particle coatings can exploit the partitioning enhancements from *kT*-scale attractive interactions to achieve relatively high mass fluxes.

The hydrodynamic resistance due to the solvent passing through macromolecular layers on particle surfaces have significant effects on diffusivities (recall Fig. 4C). Because the mass flux is proportional to permeability and thus to diffusivity, these effects can be exploited to further increase the mass flux (inset of Fig. 5C). The conversion of impermeable ($\phi = 0$, darker colors) to completely permeable ($\phi = 1$, lighter colors) increases the mass flux for both brush-only (blue) and attractive specific interactions (red) by a factor of $\sim$2.6. Thus, engineering brush-solvent permeability is a potential method for increasing overall mass flux of drug carriers.

After performing the preceding calculations of the steady state approximation to the flux (eqn (2)), the same parameters can be used in the transient concentration profiles (eqn (3)). For the same model problem, *i.e.*, particles traveling from the lung lumen through mucosal barriers into the blood (Fig. 6A), the potentials were used to calculate K and D and thus P for each particle coating at a particle size near the optimum of the flux curves, $2a = 120$ nm. The concentration profiles in the blood relative to that of the lung are plotted on semi-log scales (Fig. 6B). The particles with strongest attractive interaction reach 50% of the lung concentration after 456 s, whereas the repulsive particles would take 3528 s ($\sim$0.98 h) for the same response.

We consider next the realistic potentials and the timescales for their transport (Fig. 6C). For particles with long brushes ($L = 30$ nm) the concentration profiles reach 50% of the reference after 2442 s. For particles with *kT*-scale attractive

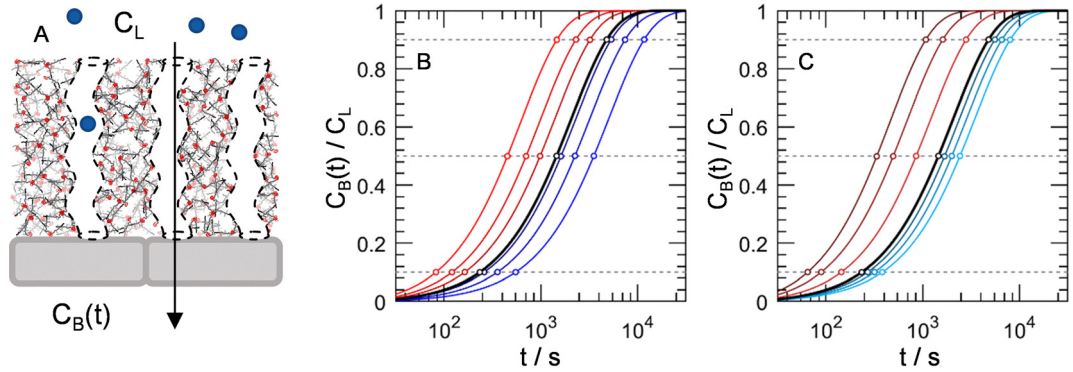

Fig. 6 Prediction of transport time through model mucus barriers. (A) Diagram of transport through the mucus barriers (grey) with C_L and $C_B(t)$. (B) and (C) Semi-log concentration series from models (eqn (3)), compared to the hard-sphere mass flux (solid black). Horizontal lines denote 10%, 50% and 90% of bolus concentration. (B) Particles with exponential potentials with the same energy scale values/color scheme as Fig. 2–4. (C) Model potentials (eqn (4)) with the same parameters/color scheme as Fig. 2–4.

interactions, the corresponding time is 336 s. There is an order of magnitude difference in times between purely repulsive brush coatings, and coatings with *kT*-scale attractions. Note also that because the longer time is comparable to the mucus clearance time, the repulsive particle coatings lead to only minimal net transport across barriers. Similarly, the attractive particles attain 10% of the reference after only 65 s, allowing for appreciable transport across even rapidly moving mucus barriers.

Enhancements from attractive interactions can lead to a roughly order-of-magnitude increase in mass flux. For these particles, the hindered transport by localization effects is counteracted by a greater enhancement of partitioning. For particles with only brush layers, the small mass flux explains the low overall effectiveness. Thus, drug transport might be optimized by enhanced partitioning even with hindered diffusivity, explaining why viruses can infect human hosts, despite having slow diffusion within barriers. Finally, rational design rules based on these mechanisms could reveal which aspects of particle surfaces lead to increased mass flux.

Design rules for maximum barrier flux

The overall flux of a drug particle formulation through the mucus barrier depends on how interactions lead to permeability and thus mass flux. Interactions govern the location and overall potential and free energy of particles within pores. Partitioning is determined by the interactions between the particle and the pore wall including hard core and surface chemistry mediated interactions. Similarly, diffusivity is determined by both the hydrodynamic and energetic interactions between the particle and pore wall, affected by localization and particle surface hydrodynamics. Permeability is the product of diffusivity and partitioning. Having considered the effects on the mass flux of different model surfaces, these effects are summarized here.

When designing drug particles, essential factors to consider include particle size, brush length, brush-solvent permeability, and the presence and strength of non-specific and specific interactions. First, the particle size affects the permeability by changing the free energy of partitioning (eqn (5)–(7)) and the hard–core hydrodynamic size for diffusion (eqn (12)). Smaller particles can transport through the barrier more effectively, but with a diminished payload. Second, brush length stabilizes particle formulations by counteracting van der Waals attraction.[89,90] However, thicker brush layers will have diminishing returns and hinder overall transport. Third, more permeable brushes improve transport, as the hydrodynamic interactions can be modified (eqn (12)) without changing spatial localization within pores. Brush layers can be engineered with different molecular constituents,[91,92] while maintaining antibiofouling characteristics.[93] Fourth, attractive interactions enhance the transport due to partitioning (eqn (9)), for interactions in the range of 0–4*kT*, which avoid irreversible adhesion.

It should be noted that these design rules are based on the underlying model assumptions. The first assumption is that mass flux depends on barrier-particle permeability, the product of partitioning and diffusivity, which is valid for particles transporting by random motion through barriers much bigger than themselves.[19] Further, the transport model is based on well understood fundamentals (see SI), meaning that optimizing the product of the two will maximize the mass flux. Maximizing partitioning or diffusion individually could lead to low overall transport. For analytical simplicity, the second assumption was of idealized pores instead of fibrous matrices. The colloidal and hydrodynamic interactions presented here correspond to spherical particles; however, the same framework could be used for flexible or non-spherical particles with appropriate corrections to interaction potentials and translational and rotational diffusivities mediated by hydrodynamic interactions. There is a lack in the literature of models and simulations of spherical particles in explicit fiber matrices, although future findings on this topic could be easily incorporated into the present fundamental transport models in the present work. However, this lack of simple matrix models makes the pore approximation for mucus[9] and hydrogel matrices[61,62] common. Despite idealized pores perhaps underestimating effects like media tortuosity or dead ends, our results show that enhanced partitioning is the dominant, engineerable effect for mass transport (Fig. 5). Finally, explicit

fibers have a distribution of pore sizes, and the mesh size does not exactly correspond to pore diameter, changing the asymptotic behavior for particles approaching the pore size. Because the partitioning effects prohibit large particles in explicit fiber models[37,46] and this model, this asymptotic regime is less important for drug delivery. It should be noted that in addition to engineering particle surfaces for optimal drug delivery, these flux predictions could be used in pharmacokinetic models for overall efficacy.

Drug particle *vs.* virus selectivity

With an understanding of the effective design of drug particles, as inspired by viruses, to maximize transport rates, it is also possible to compare drug and viral particle transport in terms of selectivity. Practically, the same model can predict the transport of both synthetic and virus particles across biological barriers, allowing for the comparison of the two (Fig. 7A). A selective barrier allows one solute through while hindering another. Selectivity is defined as the ratio of the permeabilities of two species.[15] Effective drug particles would have high mass flux, and if possible, also be transported even more efficiently than viruses. As example virus particles, we consider influenza A virus (IAV) and herpes simplex virus (HSV), for which some basic data are available.

IAV is an encapsulated virus with an approximate diameter of 120 nm.[54,94] While some IAV particles are elongated,[31] the current model does not take anisotropy into account (although it could be easily extended in future work). While anisotropy would be important for transport,[42] a first order approximation is an equivalent spherical particle. The HA/NA – sialic acid interactions have been measured directly[54] giving effective binding strengths of 1.5–2.5kT. For the middle of the range, U_M was taken to be $-2kT$ for this model. Predictions of virus particle diffusivity are comparable to the range reported recently for IAV diffusion in human airway mucus.[95]

For comparison, we first consider a drug particle design with 10 nm brushes, impermeable brush layers, and an attractive potential of $-1kT$ (blue in Fig. 7C). Due to the efficient transport of IAV particles, this virus outcompetes this drug particle design for any particle size ($\alpha = P_D/P_V < 1$). Increasing the brush length for these specific attractive interactions allow them to act over a longer range, which increases partitioning and thus permeability (green in Fig. 7C). Further, changing the brush to be more permeable to the solvent increases the diffusivity, allowing a higher permeability (orange in Fig. 7C). Only in this case is the selectivity greater than unity, albeit in a narrow range of particle sizes of 60–125 nm. Finally, increasing the strength of the specific interactions has a 3–4× factor on the overall flux (red in Fig. 7C). In that case, the region of superior selectivity by the drug particle extends to 40–240 nm, showing effective mass delivery compared to viral particles.

HSV is an enveloped spherical virus, roughly 180 nm in diameter,[9] and it forms interactions with mucin fibers that slow it down considerably although it binds reversibly.[13,96] Due to a lack of estimates for HSV binding, the same binding constants used for IAV were also used in this analysis. We again consider the same drug particle design as in Fig. 7C, with 10 nm brushes, impermeable brush layers, and an attractive

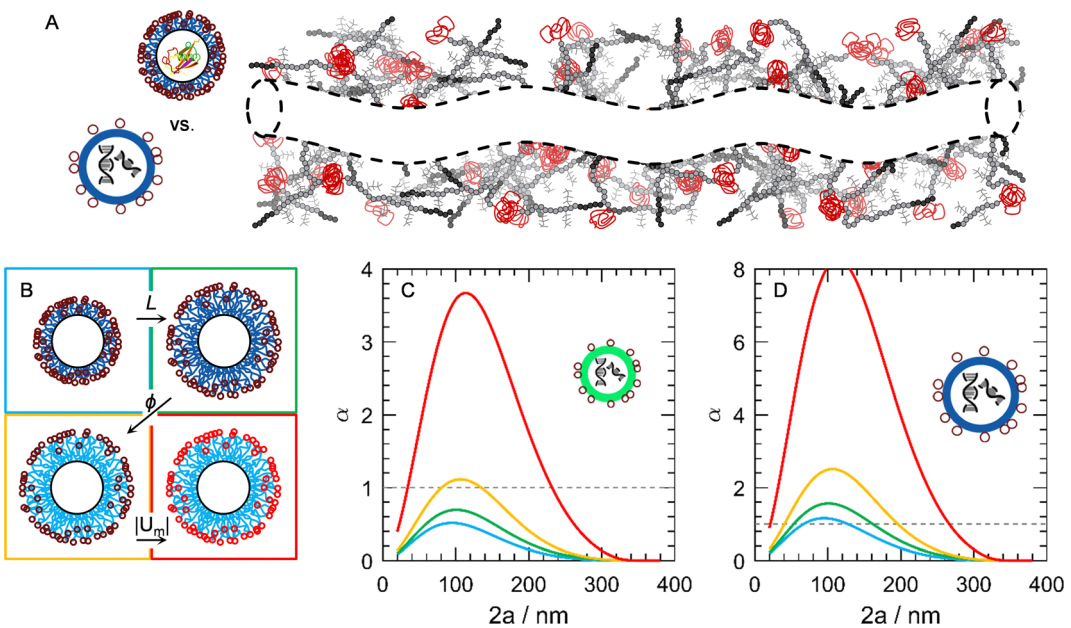

Fig. 7 Selectivity of mucus barriers to drug and viral particles. (A) Diagram of mucus pores (grey), with (top) model drug particles, with loaded insulin, poly-zwitterionic brushes (dark blue) and specific binding moieties (red), and (bottom) virus particles, with genetic material, zwitterionic lipid bilayers (blue) and proteins for specific binding (red). (B) Particle coating designs under consideration; (light blue) L = 10 nm, $U_M = -1kT$, ϕ = 0, (green) same but L = 20 nm (yellow) same but ϕ = 1 and (red) same but $U_M = -3kT$. (C) and (D) Model prediction of the selectivity of mucus barriers for drug particles over virus particles (ratios of eqn (1), $\alpha = P_D/P_V$). Drug designs are indicated with consistent colors as in panel B. Comparison of drug particles to (C) IAV particles, or (D) HSV particles.

potential of $-1kT$ (blue in Fig. 7D). This design maintains selectivity above 1 for particle sizes in a narrow range from roughly 60–125 nm. Making the same changes as in Fig. 7B, the permeability is increased sequentially with the same overall 3–4× factor increase of the mass flux (green, orange, and red in Fig. 7D). In that case, the region of enhanced drug particle selectivity extends from 20–260 nm, showing the effective mass delivery compared to viral particles.

The selectivity calculations shown here underpin the previously discussed drug particle design rules. While it is important to ensure that the particles can diffuse quickly – *e.g.*, by increasing brush length to mitigate van der Waals, or increasing brush-solvent permeability – enhancing the mass flux necessitates the optimization of the permeability, including both the diffusivity and partitioning. The net transport rate changes by roughly one order of magnitude due to enhanced partitioning (*e.g.*, Fig. 6C). In particular, the addition of specific attractive interactions could increase the efficiency of drug delivery vectors. Inspired by this, a manuscript is in preparation that directly probes virus surface inspired drug particle coatings (*i.e.*, zwitterionic polymers with boronic acid moieties capable of forming dynamic covalent bonds with sialic acids). Experiments that capture the whole transport process – *e.g.*, diffusion chambers[8] or Y-channel microfluidics (*e.g.*, see prior thesis studies[97]) – could test these predictions of enhanced mass flux in real or model mucus barriers.

Conclusions

We report a model for particle transport through biological barriers, which is used to infer design rules for surface coatings that optimize *kT*-scale interactions that mediate drug delivery, particularly for mucus barriers. Models of particle–mucus interactions include illustrative examples for electrostatic and van der Waals interactions as well as more realistic particle–pore interaction potentials based on non-specific steric interactions and specific receptor–ligand potentials. These interactions were incorporated into models for the partition and diffusion coefficients, and their product, the permeability (eqn (1)), which controls transport across mucus barriers.

Findings from the analytical model indicate several critical and dominant contributions to particle mass flux across barriers, which also determines drug mass flux carried within particles (or viruses). First, larger particles relative to pores dimensions diffusive more slowly *via* hydrodynamic interactions, which can be modified by permeable particle coatings or mucus pores, but which otherwise becomes most hindered as particle size approaches pore dimensions. Second, particle partitioning into pores is determined by several coupled contributions, including: (1) hard core particle size relative to pore dimensions that determines entropy of partitioning, which decreases from unity for infinitely small particles and vanishes as particle sizes approach pore dimensions, (2) particle–pore soft repulsion that increases effective particle size (excluded volume) to reduce partitioning relative to hard core particle dimensions, and (3) particle–pore attractive interactions that increase partitioning relative to hard core particle dimensions. Third, while particle–pore (mucus) attraction can favorably drive equilibrium portioning up to a point, attraction must be on the order of the thermal energy kT so that particles continue diffusing *via* Brownian motion driven by kT energy fluctuations; stronger attraction produces irreversible particle adhesion and clearance *via* flowing mucus barriers. Once diffusion and partitioning are maximized, the permeability can be optimized *via* choice of particle size and surface coating mediated interactions to deliver an order of magnitude increased mass flux, increasing the efficiency of small molecule drugs transport and allowing for the delivery of macromolecular cargo due to core-size constraints (*e.g.*, proteins, nucleic acids, *etc.*). Finally, the selectivity of mucus barriers to drug particle transport over virus particles is demonstrated by optimizing particle design parameters.

Ultimately, our model demonstrates a generalizable approach to the rational design of drug delivery vectors for transmucosal delivery, with broader applicability to other biological barriers. Optimizing the flux of drug particles through biological barriers requires maximization of permeability, which is the product of the diffusion and partition coefficients. Attractive specific interactions and optimizing colloidal scale hydrodynamics are strategies to enhance mass flux through barriers. These effects could increase the total mass flux by an order of magnitude.

Conflicts of interest

There are no conflicts to declare.

Data availability

Supplementary information is available. See DOI: https://doi.org/10.1039/d5sm01176k.

All data for this paper, including plots and parameters, are included within the text and figures of the manuscript.

Acknowledgements

We acknowledge financial support by the National Science Foundation 2104499 and the donors of ACS Petroleum Research Fund under 62378-ND9.

References

1 V. P. Chauhan, T. Stylianopoulos, Y. Boucher and R. K. Jain, Delivery of Molecular and Nanoscale Medicine to Tumors: Transport Barriers and Strategies, *Annu. Rev. Chem. Biomol. Eng.*, 2011, **2**, 281–298.
2 A. C. Anselmo, Y. Gokarn and S. Mitragotri, Non-Invasive Delivery Strategies for Biologics, *Nat. Rev. Drug Discovery*, 2019, **18**, 19–40.

3 J. Witten, T. Samad and K. Ribbeck, Selective Permeability of Mucus Barriers, *Curr. Opin. Biotechnol*, 2018, **52**, 124–133.
4 J. Witten and K. Ribbeck, The Particle in the Spider's Web: Transport through Biological Hydrogels, *Nanoscale*, 2017, **9**, 8080–8095.
5 L. Schoenmaker, D. Witzigmann, J. A. Kulkarni, R. Verbeke, G. Kersten, W. Jiskoot and D. J. A. Crommelin, Mrna-Lipid Nanoparticle Covid-19 Vaccines: Structure and Stability, *Int. J. Pharm.*, 2021, **601**, 120586.
6 M. J. Mitchell, M. M. Billingsley, R. M. Haley, M. E. Wechsler, N. A. Peppas and R. Langer, Engineering Precision Nanoparticles for Drug Delivery, *Nat. Rev. Drug Discovery*, 2021, **20**, 101–124.
7 R. Bansil and B. S. Turner, The Biology of Mucus: Composition, Synthesis and Organization, *Adv. Drug Delivery Rev.*, 2018, **124**, 3–15.
8 G. A. Duncan, J. Jung, J. Hanes and J. S. Suk, The Mucus Barrier to Inhaled Gene Therapy, *Mol. Ther.*, 2016, **24**, 2043–2053.
9 R. A. Cone, Barrier Properties of Mucus, *Adv. Drug Delivery Rev.*, 2009, **61**, 75–85.
10 Y.-Y. Wang, S. K. Lai, J. S. Suk, A. Pace, R. Cone and J. Hanes, Addressing the Peg Mucoadhesivity Paradox to Engineer Nanoparticles That ''Slip'' through the Human Mucus Barrier, *Angew. Chem., Int. Ed.*, 2008, **47**, 9726–9729.
11 D. Cahn and G. A. Duncan, High-Density Branched Pegylation for Nanoparticle Drug Delivery, *Cell. Mol. Bioeng.*, 2022, **15**, 355–366.
12 V. V. Khutoryanskiy, Beyond Pegylation: Alternative Surface-Modification of Nanoparticles with Mucus-Inert Biomaterials, *Adv. Drug Delivery Rev.*, 2018, **124**, 140–149.
13 S. K. Lai, Y. Y. Wang, K. Hida, R. Cone and J. Hanes, Nanoparticles Reveal That Human Cervicovaginal Mucus Is Riddled with Pores Larger Than Viruses, *Proc. Natl. Acad. Sci. U. S. A.*, 2010, **107**, 598–603.
14 C. Liu, X. Jiang, Y. Gan and M. Yu, Engineering Nanoparticles to Overcome the Mucus Barrier for Drug Delivery: Design, Evaluation and State-of-the-Art, *Med. Drug Discovery*, 2021, **12**, 100110.
15 H. B. Park, J. Kamcev, L. M. Robeson, M. Elimelech and B. D. Freeman, Maximizing the Right Stuff: The Trade-Off between Membrane Permeability and Selectivity, *Science*, 2017, **356**, eaab0530.
16 M. Kanduč, W. K. Kim, R. Roa and J. Dzubiella, How the Shape and Chemistry of Molecular Penetrants Control Responsive Hydrogel Permeability, *ACS Nano*, 2021, **15**, 614–624.
17 J. J. Keating, J. Imbrogno and G. Belfort, Polymer Brushes for Membrane Separations: A Review, *ACS Appl. Mater. Interfaces*, 2016, **8**, 28383–28399.
18 F. E. Curry and C. C. Michel, A Fiber Matrix Model of Capillary Permeability, *Microvasc. Res.*, 1980, **20**, 96–99.
19 D. J. Smith, L. G. Leal, S. Mitragotri and M. S. Shell, Nanoparticle Transport across Model Cellular Membranes: When Do Solubility-Diffusion Models Break Down?, *J. Phys. D: Appl. Phys.*, 2018, **51**, 294004.
20 S. Mitragotri, M. E. Johnson, D. Blankschtein and R. Langer, An Analysis of the Size Selectivity of Solute Partitioning, Diffusion, and Permeation across Lipid Bilayers, *Biophys. J.*, 1999, **77**, 1268–1283.
21 P. R. Johnson, N. Sun and M. Elimelech, Colloid Transport in Geochemically Heterogeneous Porous Media: Modeling and Measurements, *Environ. Sci. Technol.*, 1996, **30**, 3284–3293.
22 I. A. Kathawalla and J. L. Anderson, Pore Size Effects on Diffusion of Polystyrene in Dilute Solution, *Ind. Eng. Chem. Res.*, 1988, **27**, 866–871.
23 J. Tong and J. L. Anderson, Partitioning and Diffusion of Proteins and Linear Polymers in Polyacrylamide Gels, *Biophys. J.*, 1996, **70**, 1505–1513.
24 E. M. Johnson, D. A. Berk, R. K. Jain and W. M. Deen, Diffusion and Partitioning of Proteins in Charged Agarose Gels, *Biophys. J.*, 1995, **68**, 1561–1568.
25 J. N. Ryan and M. Elimelech, Colloid Mobilization and Transport in Groundwater, *Colloids Surf., A*, 1996, **107**, 1–56.
26 M.-S. Chun and C. Baig, Molecular Simulation Study on the Colloidal Suspension within Dilute Fibrous Media: The Effect of Particle Concentration on Partitioning, *Korean J. Chem. Eng.*, 2001, **18**, 816–823.
27 J. I. Kushner, W. M. Deen, D. Blankschtein and R. Langer, First-Principles, Structure-Based Transdermal Transport Model to Evaluate Lipid Partition and Diffusion Coefficients of Hydrophobic Permeants Solely from Stratum Corneum Permeation Experiments, *J. Pharm. Sci.*, 2007, **96**, 3236–3251.
28 J. M. Newby, I. Seim, M. Lysy, Y. Ling, J. Huckaby, S. K. Lai and M. G. Forest, Technological Strategies to Estimate and Control Diffusive Passage Times through the Mucus Barrier in Mucosal Drug Delivery, *Adv. Drug Delivery Rev.*, 2018, **124**, 64–81.
29 J. Y. Lock, T. L. Carlson and R. L. Carrier, Mucus Models to Evaluate the Diffusion of Drugs and Particles, *Adv. Drug Delivery Rev.*, 2018, **124**, 34–49.
30 T. L. Carlson, J. Y. Lock and R. L. Carrier, Engineering the Mucus Barrier, *Annu. Rev. Biomed. Eng.*, 2018, **20**, 197–220.
31 M. D. Vahey and D. A. Fletcher, Influenza a Virus Surface Proteins Are Organized to Help Penetrate Host Mucus, *eLife*, 2019, **8**, 1–24.
32 E. De Vries, W. Du, H. Guo and C. A. M. De Haan, Influenza a Virus Hemagglutinin–Neuraminidase–Receptor Balance: Preserving Virus Motility, *Trends Microbiol.*, 2020, **28**, 57–67.
33 G. I. Bell, Models for the Specific Adhesion of Cells to Cells: A Theoretical Framework for Adhesion Mediated by Reversible Bonds between Cell Surface Molecules, *Science*, 1978, **200**, 618–627.
34 A. G. Ogston, The Spaces in a Uniform Random Suspension of Fibres, *Trans. Faraday Soc.*, 1958, **54**, 1754–1757.
35 J. L. Anderson and J. A. Quinn, Restricted Transport in Small Pores: A Model for Steric Exclusion and Hindered Particle Motion, *Biophys. J.*, 1974, **14**, 130–150.
36 X. Zhu, T. J. D. Bennett, K. C. Zouboulis, D. Soulias, M. Grzybek, J. L. P. Benesch, A. H. El-Sagheer, U. Coskun

and M. Krishnan, Measurements of Molecular Size and Shape on a Chip, *Science*, 2025, **388**, 1–14.
37 J. C. Giddings, E. Kucera, C. P. Russell and M. N. Myers, Statistical Theory for the Equilibrium Distribution of Rigid Molecules in Inert Porous Networks. Exclusion Chromatography, *J. Phys. Chem.*, 1968, **72**, 4397–4408.
38 E. M. Johnson and W. M. Deen, Electrostatic Effects on the Equilibrium Partitioning of Spherical Colloids in Random Fibrous Media, *J. Colloid Interface Sci.*, 1996, **178**, 749–756.
39 K. K. S. Buck, N. I. Gerhardt, S. R. Dungan and R. J. Phillips, The Effect of Solute Concentration on Equilibrium Partitioning in Polymeric Gels, *J. Colloid Interface Sci.*, 2001, **234**, 400–409.
40 F. G. Smith and W. M. Deen, Electrostatic Effects on the Partitioning of Spherical Colloids between Dilute Bulk Solution and Cylindrical Pores, *J. Colloid Interface Sci.*, 1983, **91**, 571–590.
41 A. K. Solomon, Characterization of Biological Membranes by Equivalent Pores, *J. Gen. Physiol.*, 1968, **15**, 355–364.
42 M.-R. Rokhforouz, D. D. Sin, S. Hedtrich and J. J. Feng, Brownian Dynamics Simulation of the Diffusion of Rod-Like Nanoparticles in Polymeric Gels, *Soft Matter*, 2025, **21**, 5529–5541.
43 S. S. Datta, A. Preska Steinberg and R. F. Ismagilov, Polymers in the Gut Compress the Colonic Mucus Hydrogel, *Proc. Natl. Acad. Sci. U. S. A.*, 2016, **113**, 7041–7046.
44 J. L. Anderson, Configurational Effects on the Reflection Coefficient for Rigid Solutes in Capillary Pores, *J. Theor. Biol.*, 1981, **90**, 405–426.
45 D. E. Liu, C. Kotsmar, F. Nguyen, T. Sells, N. O. Taylor, J. M. Prausnitz and C. J. Radke, Macromolecule Sorption and Diffusion in Hema/Maa Hydrogels, *Ind. Eng. Chem. Res.*, 2013, **52**, 18109–18120.
46 Y. Cu and W. M. Saltzman, Mathematical Modeling of Molecular Diffusion through Mucus, *Adv. Drug Delivery Rev.*, 2009, **61**, 101–114.
47 R. J. Phillips, W. M. Deen and J. F. Brady, Hindered Transport in Fibrous Membranes and Gels: Effect of Solute Size and Fiber Configuration, *J. Colloid Interface Sci.*, 1990, **139**, 363–373.
48 D. Fan, S. R. Bajgiran, F. S. Samghabadi, C. Dutta, E. Gillett, P. J. Rossky, J. C. Conrad, A. B. Marciel and C. F. Landes, Imaging Heterogeneous 3d Dynamics of Individual Solutes in a Polyelectrolyte Brush, *Langmuir*, 2023, **39**, 8532–8539.
49 M. O. Ellingson and M. A. Bevan, Direct Measurements & Simplified Models of Colloidal Interactions & Diffusion with Adsorbed Macromolecules, *Soft Matter*, 2024, **20**, 6808–6821.
50 M. A. Bevan and D. C. Prieve, Hindered Diffusion of Colloidal Particles Very near to a Wall: Revisited, *J. Chem. Phys.*, 2000, **113**, 1228–1236.
51 J. H. Petropoulos, Membranes with Non-Homogeneous Sorption and Transport Properties, *Adv. Polym. Sci.*, 1985, **64**, 93–142.
52 A. R. Motezakker, L. G. Greca, E. Boschi, G. Siqueira, F. Lundell, T. Rosén, G. Nyström and L. Söderberg, Stick, Slide, or Bounce: Charge Density Controls Nanoparticle Diffusion, *ACS Nano*, 2024, **18**, 28636–28648.
53 W. N. Everett, D. J. Beltran-Villegas and M. A. Bevan, Concentrated Diffusing Colloidal Probes of Ca2+-Dependent Cadherin Interactions, *Langmuir*, 2010, **26**, 18976–18984.
54 L. Kaler, E. Iverson, S. Bader, D. Song, M. A. Scull and G. A. Duncan, Influenza A Virus Diffusion through Mucus Gel Networks, *Commun. Biol.*, 2022, **5**, 1–9.
55 W. N. Everett, H.-J. Wu, S. G. Anekal, H.-J. Sue and M. A. Bevan, Diffusing Colloidal Probes of Protein and Synthetic Macromolecule Interactions, *Biophys. J.*, 2007, **92**, 1005–1013.
56 D. Tian, Z. Qu, T. Lai and G. Zhu, A Prediction Model for Nanoparticle Diffusion Behavior in Fibrous Materials Considering Steric and Hydrodynamic Resistances, *Phys. Chem. Chem. Phys.*, 2022, **24**, 24394–24403.
57 P. G. de Gennes, Reptation of a Polymer Chain in the Presence of Fixed Obstacles, *J. Chem. Phys.*, 1971, **55**, 572–579.
58 S. F. Edwards, The Statistical Mechanics of Polymerized Material, *Proc. Phys. Soc.*, 1967, **92**, 9.
59 M. Doi and S. F. Edwards, Dynamics of Concentrated Polymer Systems. Part 1.—Brownian Motion in the Equilibrium State, *J. Chem. Soc., Faraday Trans. 2*, 1978, **74**, 1789–1801.
60 N. Fakhri, F. MacKintosh, B. Lounis, L. Cognet and M. Pasquali, Brownian Motion of Stiff Filaments in a Crowded Environment, *Science*, 2010, **330**, 1804–1807.
61 M. Smith, R. Poling-Skutvik, A. H. Slim, R. C. Willson and J. C. Conrad, Dynamics of Flexible Viruses in Polymer Solutions, *Macromolecules*, 2021, **54**, 4557–4563.
62 F. Safi Samghabadi, A. H. Slim, M. W. Smith, M. Chabi and J. C. Conrad, Dynamics of Filamentous Viruses in Polyelectrolyte Solutions, *Macromolecules*, 2022, **55**, 10694–10702.
63 Y. Pawar and J. L. Anderson, Hindered Diffusion in Slit Pores: An Analytical Result, *Ind. Eng. Chem. Res.*, 1993, **32**, 743–746.
64 P. Ganatos, S. Weinbaum and R. Pfeffer, A Strong Interaction Theory for the Creeping Motion of a Sphere between Plane Parallel Boundaries. Part 2. Parallel Motion, *J. Fluid Mech.*, 1980, **99**, 739–753.
65 P. Ganatos, S. Weinbaum and R. Pfeffer, A Strong Interaction Theory for the Creeping Motion of a Sphere between Plane Parallel Boundaries. Part 1. Perpendicular Motion, *J. Fluid Mech.*, 1980, **99**, 739–753.
66 S. L. Eichmann and M. A. Bevan, Direct Measurements of Protein-Stabilized Gold Nanoparticle Interactions, *Langmuir*, 2010, **26**, 14409–14413.
67 S. L. Eichmann, S. G. Anekal and M. A. Bevan, Electrostatically Confined Nanoparticle Interactions and Dynamics, *Langmuir*, 2008, **24**, 714–721.
68 W. M. Deen, Hindered Transport of Large Molecules in Liquid-Filled Pores, *AIChE J.*, 1987, **33**, 1409–1425.
69 H. Brenner and L. J. Gaydos, The Constrained Brownian Movement of Spherical Particles in Cylindrical Pores of Comparable Radius: Models of the Diffusive and Convective

Transport of Solute Molecules in Membranes and Porous Media, *J. Colloid Interface Sci.*, 1977, **58**, 312–356.
70 G. M. Mavrovouniotis and H. Brenner, Hindered Sedimentation, Diffusion, and Dispersion Coefficients for Brownian Spheres in Circular Cylindrical Pores, *J. Colloid Interface Sci.*, 1988, **124**, 269–283.
71 J. Happel and H. Brenner, *Low Reynolds Number Hydrodynamics*, Prentice-Hall, Englewood Cliffs, NJ, 1965.
72 M. Cohen, X.-Q. Zhang, H. P. Senaati, H.-W. Chen, N. M. Varki, R. T. Schooley and P. Gagneux, Influenza a Penetrates Host Mucus by Cleaving Sialic Acids with Neuraminidase, *Virol. J.*, 2013, **10**, 321.
73 R. Bansil and B. S. Turner, Mucin Structure, Aggregation, Physiological Functions and Biomedical Applications, *Curr. Opin. Colloid Interface Sci.*, 2006, **11**, 164–170.
74 H.-J. Wu and M. A. Bevan, Direct Measurement of Single and Ensemble Average Particle-Surface Potential Energy Profiles, *Langmuir*, 2005, **21**, 1244–1254.
75 M. O. Ellingson and M. A. Bevan, Kt- & Fn- Scale Polymer Brush Interactions: Theory Vs. Experiment for Aqueous Polyethylene Glycol Layers, *Macromolecules*, 2025, **58**, 9044–9054.
76 G. A. Duncan and M. A. Bevan, Colloidal Potentials Mediated by Specific Biomolecular Interactions, *Soft Matter*, 2014, **10**, 8524–8532.
77 S. L. Eichmann, G. Meric, J. C. Swavola and M. A. Bevan, Diffusing Colloidal Probes of Protein–Carbohydrate Interactions, *Langmuir*, 2013, **29**, 2299–2310.
78 L. R. White, On the Deryaguin Approximation for the Interaction of Macrobodies, *J. Colloid Interface Sci.*, 1983, **95**, 286–288.
79 J. C. Swavola, T. D. Edwards and M. A. Bevan, Direct Measurement of Macromolecule-Coated Colloid-Mucus Interactions, *Langmuir*, 2015, **31**, 9076–9085.
80 Q. Xu, L. M. Ensign, N. J. Boylan, A. Schön, X. Gong, J.-C. Yang, N. W. Lamb, S. Cai, T. Yu, E. Freire and J. Hanes, Impact of Surface Polyethylene Glycol (Peg) Density on Biodegradable Nanoparticle Transport in Mucus Ex Vivo and Distribution in Vivo, *ACS Nano*, 2015, **9**, 9217–9227.
81 J. Israelachvili, Differences between Non-Specific and Bio-Specific, and between Equilibrium and Non-Equilibrium, Interactions in Biological Systems, *Q. Rev. Biophys.*, 2005, **38**, 331–337.
82 K. E. Cureno-Hernandez, J. Lee, S. Kim, Z. Cartwright and M. Herrera-Alonso, Boronic Acid-Mediated Mucin/Surface Interactions of Zwitterionic Polymer Brushes, *Soft Matter*, 2025, **21**, 3125–3136.
83 J. A. Barrie, H. G. Spencer and A. Quig, Transient Diffusion through a Membrane Separating Finite and Semi-Infinite Volumes, *J. Chem. Soc., Faraday Trans. 1*, 1975, **71**, 2459–2467.
84 S. Bhattacharjee and A. Sharma, Lifshitz-van der Waals Energy of Spherical Particles in Cylindrical Pores, *J. Colloid Interface Sci.*, 1995, **171**, 288–296.
85 G. A. Duncan and M. A. Bevan, Computational Design of Nanoparticle Drug Delivery Systems for Selective Targeting, *Nanoscale*, 2015, **7**, 15332–15340.
86 T. C. Laurent and J. Killander, A Theory of Gel Filtration and Its Experimental Verification, *J. Chromatogr. A*, 1964, **14**, 317–330.
87 J. Happel and H. Brenner, *Low Reynolds Number Hydrodynamics: With Special Applications to Particulate Media*, Martinus Nijhoff Publishers, Boston, 1983.
88 A. J. Goldman, R. G. Cox and H. Brenner, Slow Viscous Motion of a Sphere Parallel to a Plane Wall – I Motion through a Quiescent Fluid, *Chem. Eng. Sci.*, 1967, **22**, 637–651.
89 M. Zhang, B. P. Bishop, N. L. Thompson, K. Hildahl, B. Dang, O. Mironchuk, N. Chen, R. Aoki, V. C. Holmberg and E. Nance, Quantum Dot Cellular Uptake and Toxicity in the Developing Brain: Implications for Use as Imaging Probes, *Nanoscale Adv.*, 2019, **1**, 3424–3442.
90 C. Curtis, D. Toghani, B. Wong and E. Nance, Colloidal Stability as a Determinant of Nanoparticle Behavior in the Brain, *Colloids Surf., B*, 2018, **170**, 673–682.
91 S. Feng, Y. Liu, J. Li and S. Wen, Superlubricity Achieved with Zwitterionic Brushes in Diverse Conditions Induced by Shear Actions, *Macromolecules*, 2021, **54**, 5719–5727.
92 M. Chen, W. H. Briscoe, S. P. Armes and J. Klein, Lubrication at Physiological Pressures by Polyzwitterionic Brushes, *Science*, 2009, **323**, 1698–1701.
93 G. S. Georgiev, E. B. Kamenska, E. D. Vassileva, I. P. Kamenova, V. T. Georgieva, S. B. Iliev and I. A. Ivanov, Self-Assembly, Antipolyelectrolyte Effect, and Nonbiofouling Properties of Polyzwitterions, *Biomacromolecules*, 2006, **7**, 1329–1334.
94 J. Vajda, D. Weber, D. Brekel, B. Hundt and E. Müller, Size Distribution Analysis of Influenza Virus Particles Using Size Exclusion Chromatography, *J. Chromatogr. A*, 2016, **1465**, 117–125.
95 L. Kaler, K. Joyner and G. A. Duncan, Machine Learning-Informed Predictions of Nanoparticle Mobility and Fate in the Mucus Barrier, *APL Bioeng.*, 2022, **6**, 026103.
96 S. S. Olmsted, J. L. Padgett, A. I. Yudin, K. J. Whaley, T. R. Moench and R. A. Cone, Diffusion of Macromolecules and Virus-Like Particles in Human Cervical Mucus, *Biophys. J.*, 2001, **81**, 1930–1937.
97 J. C. Swavola, *Conservative and Dissipative Force Measurement to Engineer Stealth Drug Delivery Particles*, Johns Hopkins, Baltimore, MD, 2014.

